

Journal of Materials Chemistry C

Accepted Manuscript



This is an *Accepted Manuscript*, which has been through the Royal Society of Chemistry peer review process and has been accepted for publication.

Accepted Manuscripts are published online shortly after acceptance, before technical editing, formatting and proof reading. Using this free service, authors can make their results available to the community, in citable form, before we publish the edited article. We will replace this *Accepted Manuscript* with the edited and formatted *Advance Article* as soon as it is available.

You can find more information about *Accepted Manuscripts* in the [Information for Authors](#).

Please note that technical editing may introduce minor changes to the text and/or graphics, which may alter content. The journal's standard [Terms & Conditions](#) and the [Ethical guidelines](#) still apply. In no event shall the Royal Society of Chemistry be held responsible for any errors or omissions in this *Accepted Manuscript* or any consequences arising from the use of any information it contains.

BaGa₂SnSe₆: A New Phase-Matchable IR Nonlinear Optical Material with Strong Second Harmonic Generation Response

Xiaoshuang Li,^{abc} Chao Li,^{abc} Pifu Gong,^{abc} Zheshuai Lin,^{ab} Jiyong Yao,^{*ab} and Yicheng Wu^{ab}

By introducing heavy Sn ion to Ba-Ga-Q system, a new IR nonlinear optical material BaGa₂SnSe₆ has been obtained. It crystallizes in space group *R*3 of the trigonal system, with $a = 10.1449(14)$ Å, $c = 9.2490(18)$ Å, and $Z = 3$. In the structure, three (Ga/Sn)Se₄ are connected via corner-sharing to generate (Ga/Sn)₃Se₉ building groups, which are further joined to produce three-dimensional network with Ba²⁺ lying in the cavities. Due to the contribution of the large and easily-polarizable Sn atom and the polar arrangements of the (Ga/Sn)Se₄ tetrahedra, the compound exhibits a very strong NLO response that is ~5.2 times that of the benchmark AgGaS₂ at a fundamental laser radiation of 2.09 μm, and shows type-I phase-matchable behavior. Furthermore, the calculated birefringence index is $\Delta n = 0.1649$ at 1.064 μm and the major SHG tensors are $d_{11} = 62.91$ pm/V and $d_{33} = 50.26$ pm/V.

^a Center for Crystal Research and Development, Technical Institute of Physics and Chemistry, Chinese Academy of Sciences, Beijing 100190, P.R. China, Email: jyao@mail.ipc.ac.cn

^b Key Laboratory of Functional Crystals and Laser Technology, Chinese Academy of Sciences, Beijing 100190, P.R. China

^c University of Chinese Academy of Sciences, Beijing 100049, P.R. China

†Electronic supplementary information (ESI) available: Crystallographic data in CIF format for BaGa₂SnSe₆. CCDC number: 1416205.

Introduction

Due to their laser frequency conversion properties, nonlinear optical (NLO) crystals are a very important class of optoelectronic material.¹⁻⁹ In the past decades, several outstanding NLO crystals have largely satisfied the urgent need of UV and visible NLO applications. However, in infrared (IR) region, only a few NLO crystals (e.g., chalcopyrite-type AgGaQ_2 ($\text{Q} = \text{S}, \text{Se}$) and ZnGeP_2) are commercially available to date, and each of them suffers from drawbacks that severely limit their wider application.¹⁰⁻¹⁴ As a consequence, the exploration for new IR NLO materials with better overall properties is extremely urgent. The desirable properties for an IR NLO materials include: (1) a large NLO coefficient to increase the energy conversion efficiency. (2) sufficiently large birefringence (Δn) to satisfy the phase matching requirement. (3) wide IR transparency region. (4) high laser induced damage threshold. (5) good chemical and thermal stability.¹⁵

During the last decades, researches were widely carried out on metal chalcogenides,¹⁶⁻²³ a rich source of IR nonlinear optical materials.²⁴⁻⁴⁰ Compared with oxides, metal chalcogenides have much boarder IR transmission range and hence are more suitable for IR NLO application. An effective way to achieve large NLO response and large birefringence is to introduce heavy atoms because the more electrons the center cations have, the easier the NLO-active anionic groups are to be polarized, which in turn may enhance the NLO responses and the birefringence. For example, BaGa_4Se_7 ²⁶ demonstrates four-five times larger SHG response than the isostructural BaAl_4Se_7 ⁴⁰. Previously, we identified BaGa_2MQ_6 ($\text{M} = \text{Si}, \text{Ge}$; $\text{Q} = \text{S},$

Se)³⁶, which show excellent overall properties for practical applications. Here we are interested in introducing the heavy and easily-polarizable Sn atom to replace Si and Ge atoms, hoping to further increase the NLO coefficients and birefringence. Our efforts have led to the discovery of a new quaternary IR NLO material BaGa₂SnSe₆ with impressive NLO property. In this paper, we report the synthesis, crystal structure, thermal, optical property, and theoretical calculation of this material.

Experimental section

Reagents.

The following reagents were used as obtained: Ba (99.9%), Ga (99.99%), Sn (99.99%), S (99.9999%), BaS (98%) and Se (99.9999%), all from Sinopharm. The binary starting materials, BaSe, Ga₂Q₃, and SnQ₂ were synthesized by the stoichiometric reactions of elements at high temperatures in sealed silica tubes evacuated to 10⁻³Pa.

Synthesis.

The mixtures of BaQ, Ga₂Q₃, and SnQ₂ in molar ratios of 1:1:1, 6:1:2, 2:3:2, and 2:1:6 were ground and loaded into fused-silica tubes under an Ar atmosphere in a glovebox. The tubes were flame sealed under a high vacuum of 10⁻³ Pa and then placed in a computer-controlled furnace. The samples were heated to 1273 K in 24 h and kept at that temperature for 48 h, then cooled at a slow rate of 3 K/h to 623 K, and finally cooled to room temperature naturally. Yellow and red crystals were obtained.

Analyses of the crystals with an EDX-equipped Hitachi S-4800 SEM and single crystal X-ray diffraction revealed the previously reported BaGa₂Q₄ and BaGa₄Q₇ as major products in all sulfide reactions and the three selenide reactions with the starting material compositions of BaQ : Ga₂Q₃ : SnQ₂ = 1:1:1, 6:1:2, 2:3:2. Encouragingly, a new quaternary compounds with Ba, Ga, Sn, and Se in the approximate ratio of 1:2:1:6 was found in products of the reaction with starting materials BaSe : Ga₂Se₃ : SnSe₂ = 2:1:6, and the yield in our reaction was ~50%, based on Ga. The red BaGa₂SnSe₆ crystal is of good quality and stable in the air for months.

Structure Determination.

Single-crystal X-ray diffraction data of BaGa₂SnSe₆ were collected with the use of graphite-monochromatized Mo K α ($\lambda = 0.71073 \text{ \AA}$) at 153 K on a Rigaku AFC10 diffractometer equipped with a Saturn CCD detector. Crystal decay was monitored by re-collecting 50 initial frames at the end of data collection. The collection of the intensity data, cell refinement and data reduction were carried out with the use of the program Crystalclear.⁴¹ Face-indexed absorption corrections were performed numerically with the use of the program XPREP.⁴²

The structure was solved with the direct methods program SHELXS and refined with the least-squares program SHELXL of the SHELXTL.PC suite of programs.⁴² The atomic assignment and structural refinement were performed in similar manner as the BaGa₂MQ₆ (M = Si, Ge; Q = S, Se)³⁶ compounds except that the tetrahedral

position is randomly occupied by the Ga and Sn atoms with refined occupancy of Ga:Sn = 2:1, which is close to the EDX measurement results. The atomic coordinates are now standardized with the program TIDY.⁴³ The final refinement included anisotropic displacement parameters and a secondary extinction correction. Additional experimental details are given in Table 1 and selected metrical data are given in Table 2. Further information may be found in the Supporting Information.

Powder X-ray Diffraction.

Single crystals of BaGa₂SnSe₆ (about 0.3 g) were hand-picked from reaction products and ground to powder. Then the powder X-ray diffraction (PXRD) pattern of the powder sample was collected on a Rigaku MiniFlex II diffractometer (Cu K α radiation, $\lambda = 1.5406 \text{ \AA}$) at 293 K. The 2θ range is 10–70 °, with a step size of 0.02 ° and a scan speed of 0.1 s/step. PXRD pattern (Fig. 1) agrees well with the simulated pattern generated using the CIF of the refined single crystal structure data (153K), indicating that BaGa₂SnSe₆ does not undergo structural change from 153 K to 293 K and that the bulk sample is of high purity.

Thermal Analysis.

A LabsysTMTG-DTA16 (SETARAM) thermal analyzer was used to investigate the thermal property by the differential scanning calorimetric (DSC) analysis (the DSC was calibrated with Al₂O₃). About 15 mg of the BaGa₂SnSe₆ sample was placed in a silica tube (5 mm o.d. \times 3 mm i.d.) and subsequently sealed under a high vacuum. The

heating and the cooling rates were both 15 K/min.

UV–vis–NIR Diffuse Reflectance Spectroscopy.

A Cary 5000 UV-vis-NIR spectrophotometer with a diffuse reflectance accessory was used to measure the spectrum of BaGa₂SnSe₆ and BaSO₄ as a reference in the range 250 nm (5.0 eV) to 2500 nm (0.5 eV).

SHG Measurement.

The optical SHG response of BaGa₂SnSe₆ was measured by means of the Kurtz-Perry method.⁴⁴ The fundamental light is the 2.09 μm light generated with a Q-switched Ho:Tm:Cr:YAG laser. The BaGa₂SnSe₆ crystals were hand-picked and ground to powder with the particle size ranging from 20 to 150 μm for the measurement and AgGaS₂ sieved in the size 105–150 μm was used as a reference.

Calculated Method.

The first-principles calculations for BaGa₂SnSe₆ were performed by the plane-wave pseudopotential method implemented in the CASTEP package.⁴⁵ In order to calculate the disordered structure, one ordered structure was used in which the three statistical locations were occupied by one Sn and two Ga atoms, respectively. The ion-electron interactions were modeled by the ultrasoft pseudopotentials⁴⁶ for all elements. The local density approximation (LDA)⁴⁷ was adopted to describe the exchange and correlation (XC) potentials. The kinetic energy cutoffs of 350 eV and Monkhorst-Pack

k -point meshes⁴⁸ with a density of $(3 \times 3 \times 3)$ points in the Brillouin zone were chosen.

It is well acknowledged that the DFT calculations with the XC functional always underestimate the energy band gap of crystals. For calculating the optical coefficients, a scissors operator^{49, 50} is usually introduced to shift up all the conduction bands to agree with the measured band gap. Then based on the electronic structures, the second-order susceptibility $\chi^{(2)}$, i.e., the SHG coefficient d_{ij} , can be calculated.⁵¹

Results and discussion

Synthesis.

Interestingly, BaGa₂SnSe₆ was not obtained from the stoichiometric reaction but with the excessive SnSe₂ (melting point 948 K) probably as flux, which was also identified in the reaction product. The Sn flux method was used in the synthesis of Cu₃SbSe₄,⁵² MoS₂,⁵³ and La_{1-x}Nd_xCo₂P₂.⁵⁴ Although the synthesis of metal chalcogenides from SnSe₂ flux is not common, the preparation of BaGa₂SnSe₆ from SnSe₂ flux may open a way to further synthetic exploration of metal chalcogenides. Great efforts have been made to synthesize analogues in Ba-Ga-Sn-S system, but they did not work after many trials. Thus, we only report the study on BaGa₂SnSe₆ here.

Crystal Structure.

BaGa₂SnSe₆ crystallizes in the noncentrosymmetric polar space group $R\bar{3}$ of the trigonal system, with $a = 10.1449(14)$ Å, $c = 9.2490(18)$ Å, and $Z = 3$. In the

asymmetric unit, there is one crystallographically independent Ba atom, one metal position randomly occupied by both Ga and Sn in the molar ratio of 2:1, and two Se atoms. Because there are no Se–Se bonds in the structures, the oxidation states of 2+, 3+, 4+, and 2– can be assigned to Ba, Ga, Sn, and Se, respectively.

As shown in Fig. 2A, the Ga/Sn atoms are 4-fold coordinated by four Se atoms in distorted tetrahedra with (Ga/Sn)–Se bond lengths ranging from 2.355(7) to 2.4501(7) Å (Table 3), a bit shorter than (Ga/Sn)–Se bond distances of 2.421 (2) to 2.482 (2) Å in $\text{Na}_{0.3}\text{Ga}_{0.9}\text{Sn}_{0.6}\text{Se}_3$,⁵⁵ and 2.423(1) to 2.522(1) Å in KGaSnSe_4 .⁵⁵ Besides, (Ga/Sn)–Se bond lengths in the title compound are also a little smaller than typical Sn–Se values of 2.516(1) to 2.525(1) Å in $\text{K}_2\text{MnSn}_2\text{Se}_6$,⁵⁶ and 2.479(5) to 2.968(7) Å in $\text{Ba}_6\text{Ga}_2\text{SnSe}_{11}$.⁵⁷ Furthermore, the Ba atoms in this compound are surrounded by twelve Se atoms with Ba–Se interatomic distances varying from 3.5891(9) to 3.8131(9) Å, which are a little longer to those observed in related compounds, such as $\text{Ba}_6\text{Ga}_2\text{SnSe}_{11}$ (3.266(1) to 3.746(1) Å),⁵⁷ and $\text{Ba}_4\text{CuGa}_5\text{Se}_{12}$ (3.289(1) to 3.618 (1) Å).⁵⁸

The structure of $\text{BaGa}_2\text{SnSe}_6$ is illustrated in Fig. 2. As is in the case of BaGa_2MQ_6 (M = Si, Ge; Q = S, Se)³⁶, $(\text{Ga/Sn})_3\text{Se}_9$ group ring is the fundamental building unit of $\text{BaGa}_2\text{SnSe}_6$ (Fig. 2A). The $(\text{Ga/Sn})_3\text{Se}_9$ groups are arranged in parallel manners and completely isolated from each other in the *ab* plane (Fig. 2B), and are further linked with each other via sharing Se1 atoms along the *c* direction to generate the three-dimensional framework with Ba^{2+} cations locating in the cavities (Fig. 2C). Nevertheless, due to the introduction of the large Sn atom, $\text{BaGa}_2\text{SnSe}_6$

possess the obviously larger cell volume ($824.4(2) \text{ \AA}^3$) than the other two selenides of $\text{BaGa}_2\text{SiSe}_6$ ($778.3(2) \text{ \AA}^3$) and $\text{BaGa}_2\text{GeSe}_6$ ($788.4(2) \text{ \AA}^3$).

Another series of compounds with similar stoichiometry were also reported, namely AGa_2MQ_6 ($\text{A} = \text{Sn}, \text{M} = \text{Ge}, \text{Q} = \text{S}; \text{A} = \text{Pb}, \text{M} = \text{Si}, \text{Ge}; \text{Q} = \text{Se}$)^{39, 59}. Although $\text{BaGa}_2\text{SnSe}_6$ possesses the same stoichiometry as the AGa_2MQ_6 ($\text{A} = \text{Sn}, \text{M} = \text{Ge}, \text{Q} = \text{S}; \text{A} = \text{Pb}, \text{M} = \text{Si}, \text{Ge}; \text{Q} = \text{Se}$) compounds, they crystallize in three different space groups ($R3$ for $\text{BaGa}_2\text{SnSe}_6$, $Fdd2$ for $\text{SnGa}_2\text{GeSe}_6$, $\text{PbGa}_2\text{GeSe}_6$, and Cc for $\text{PbGa}_2\text{SiSe}_6$). For $\text{BaGa}_2\text{SnSe}_6$, the Ba–Se interaction is mostly ionic in character with no orientational preference, leading to a more “spherical” coordination environment for Ba. Consequently, the three-dimensional framework in $\text{BaGa}_2\text{SnSe}_6$ is formed by the $(\text{Ga}/\text{Sn})\text{Se}_4$ tetrahedra only. However, for AGa_2MQ_6 ($\text{A} = \text{Sn}, \text{M} = \text{Ge}, \text{Q} = \text{S}; \text{A} = \text{Pb}, \text{M} = \text{Si}, \text{Ge}; \text{Q} = \text{Se}$), Sn and Pb are covalently-coordinated to five or four Se atoms owing to the stereochemical activity of the lone pair electrons. And the distorted SnS_5 and PbSe_4 polygonal-pyramids are joined to MSe_4 ($\text{M} = \text{Ga}, \text{Si}, \text{Ge}$) alternately forming chains along b direction, which in turn become a part of the three-dimensional framework.

Interestingly, changing the tetravalent ions did not result in the changes of structure types in the series of $\text{BaGa}_2\text{MSe}_6$ ($\text{M} = \text{Si}, \text{Ge}, \text{Sn}$), while there is a phase transition from the monoclinic space group Cc to the orthorhombic space group $Fdd2$, when Si was replaced by Ge in the series of $\text{PbGa}_2\text{MSe}_6$ ($\text{M} = \text{Si}, \text{Ge}$). This phenomenon demonstrates that the structure-directing natures of ionic Ba and covalent Pb are obviously different. Thus, taking advantage of the different effects of

structure-directing cations and the connection flexibility of MSe_4 tetrahedra could result in an impressive structural diversity, which may provide an enormous playground for a further fundamental understanding of the synthetic methods and the composition-structure-property relationship of metal chalcogenides.

Thermal Analysis.

The DSC curve of this compound is shown in Fig. 3. It is evident that $BaGa_2SnSe_6$ has an endothermic peak at 923 K, and two exothermic peaks at 974 and 872 K, which indicates the crystal melts incongruently, corresponding to the Sn-flux synthesis method. In comparison, the melting points are 1271 K for $AgGaS_2$, 1133 K for $AgGaSe_2$, 1298 K for $ZnGeP_2$, 1361 K for $BaGa_4S_7$, and 1241 K for $BaGa_4Se_7$. The rather low melting point of $BaGa_2SnSe_6$ may help to decrease the vapor pressure during crystal growth.

Optical property.

The optical diffuse reflectance method was used for the determination of the band gap. Based on the UV–Vis–NIR diffuse–reflectance spectrum, absorption ($F(R)$) data are calculated from the following Kubelka–Munk function (1):^{60, 61}

$$F(R) = \frac{K}{S} = \frac{(1-R)^2}{2R} \quad (1)$$

where R is the reflectance, K is the absorption, and S is the scattering. As shown in Fig. 4, experimental band gap of $BaGa_2SnSe_6$ is 1.95 eV, consistent with the red color of the compound. This band gap is obviously smaller than that of the related isostructural

BaGa₂SiSe₆ (2.88 eV) and BaGa₂GeSe₆ (2.22 eV) compounds.³⁶ It is evident that the involvement of heavier tetravalent ion tends to decrease the band gaps in this series of compounds as the valence orbitals of the tetravalent ions contribute to the bottom of the conduction bands to large extent and the energy of these valence orbitals decreases from Si to Ge and to Sn. Alternatively, the band gap differences can be viewed as heavily influenced by the different electron binding capacities of the atomic kernel. The weaker the electron binding capacities of the atomic kernel are, the smaller the band gaps will be. Obviously, from Si to Sn, the atomic radii become larger and larger, resulting in the weakening of electron binding capacities of the atomic kernel. As a consequence, their band gaps decrease from Si to Sn: BaGa₂SiSe₆ > BaGa₂GeSe₆ > BaGa₂SnSe₆.

To correctly determine the IR transmission range of the compound, large-size single crystal is needed. Unfortunately, the sizes of the tiny crystals in our synthesis lie in micrometers even after several trials. As a result, the IR transparent spectrum is not measured. Still, from extensive research on numerous IR NLO materials including AgGaQ₂ (Q = S, Se)^{10, 15} and BaGa₄Q₇ (Q = S, Se)^{25, 26} IR materials, chalcogenides have much broader IR transparent range than oxides (up to 12 μm for sulfides, and up to 18 μm for selenides). Hence, as a selenide, BaGa₂SnSe₆ should be able to cover the two atmospheric windows of “3–5 μm” and “8–12 μm”.

NLO Property.

The ternary chalcopyrite AgGaS₂ has been widely used as benchmark material for

decades, due to its good properties, such as high SHG coefficient (d_{36}) (13.7 pm/V), wide transparent region (0.5–13 μm), relatively large birefringence, and easy availability.¹⁵ As shown in Fig. 5, the SHG intensity of $\text{BaGa}_2\text{SnSe}_6$ increases with the increase in particle size. Although the curve does not reach a platform due to the lacking of larger size particles, the increasing SHG intensity with the larger particle size and calculated birefringence (0.1649 at 1.064 μm and 0.1473 at 2.0 μm) indicates that $\text{BaGa}_2\text{SnSe}_6$ could achieve the type-I PM in the MIR region.^{26, 62} Furthermore, the powder SHG signal intensity of $\text{BaGa}_2\text{SnSe}_6$ is ~ 5.2 times that of the commercial AgGaS_2 at a particle size of 105–150 μm (Fig. 6).

In this structure, $(\text{Ga}/\text{Sn})\text{Se}_4$ units are the microscopic NLO-active building blocks. As shown in Fig. 2B, all $(\text{Ga}/\text{Sn})\text{Se}_4$ tetrahedra are polarized in the same direction c . Such polar arrangements are responsible for the large second harmonic generation (SHG) response observed. In addition, due to the presence of the large and polarizable Sn atom, $\text{BaGa}_2\text{SnSe}_6$ exhibits much stronger SHG response than the isostructural BaGa_2MQ_6 ($\text{M} = \text{Si}, \text{Ge}; \text{Q} = \text{S}, \text{Se}$)³⁶ compounds, among which the largest the SHG signal intensity is ~ 3.5 AgGaS_2 for $\text{BaGa}_2\text{GeSe}_6$. The more diffuse nature of the electron orbital of Sn makes the SnSe_4 tetrahedra more susceptible to polarization, leading to the stronger NLO response of $\text{BaGa}_2\text{SnSe}_6$.

Theoretical Results.

A. Electronic structures and properties.

Fig. 7A shows the electronic band structure of $\text{BaGa}_2\text{SnSe}_6$ along the lines of high

symmetry points in the Brillouin zone. It is clear that BaGa₂SnSe₆ is a direct gap crystal with a calculated band gap of 1.6 eV. The partial density of state (PDOS) projected on the constitutional atoms of BaGa₂SnSe₆ is shown in Fig. 7B, from which several electronic characteristics are shown: (i) The valence band (VB) lower than -5eV are mainly consisted of the isolated inner-shell orbitals of Ba *6s5p*, Ga *4s3d*, Sn *5s* and Se *4s*, which have little interaction with neighbor atoms; (ii) The upper part of VB and the bottom of CB are mainly composed of the *p* orbitals of Ga (*4p*) Sn (*5p*) and Se (*4p*), thus the states on the both sides of the band gap mostly consist of those from the Ga/Sn-Se group. Since the optical response of a crystal mainly originates from the electronic transitions between the VB and CB states close to the band gap,⁶³ the Ga/Sn-Se group determine the optical properties in the crystal.

B. Optical response

The nonlinear and linear optical properties were investigated by the scissors factors corrected LDA approach and the results are listed in Table 3 and Table 4. As shown, the largest and the average powder SHG coefficients are 62.91 and 40.06 pm/V respectively, in good accordance with the experimental results. The birefringence (Δn) is 0.1649 at the wavelength of 1.064 μm and 0.1473 at 2.090 μm , indicating that this compound is easy to achieve the phase-matching condition in the IR spectral region. In comparison, the largest SHG coefficient and the birefringence at 1 μm and 2 μm for BaGa₂SiSe₆ and BaGa₂GeSe₆ are -15.3 pm/V, 0.07, 0.07 and -27.4 pm/V, 0.15, 0.13 respectively. It is interesting that BaGa₂SnSe₆ has the largest SHG coefficients and birefringence in these three compounds, which is mainly because of the (Ga/Sn)Se₄

tetrahedron exhibiting the largest polarizability among the three compounds.

Conclusions

In summary, a quaternary IR NLO chalcogenide $\text{BaGa}_2\text{SnSe}_6$ has been synthesized and characterized. Its structure is constructed by corner sharing $(\text{Ga}/\text{Sn})\text{Se}_4$ units with 12-fold coordinated Ba residing in the cavities. The compound exhibits a very strong NLO response that is ~ 5.2 times as large as that of the benchmark AgGaS_2 at a laser radiation of $2.09 \mu\text{m}$, and type-I PM behavior. The NLO response mainly originates from $(\text{Ga}/\text{Sn})\text{Se}_4$ tetrahedra in the polar arrangement. Clearly, the big difference of NLO responses among $\text{BaGa}_2\text{SnSe}_6$, $\text{BaGa}_2\text{GeSe}_6$, and $\text{BaGa}_2\text{SiSe}_6$ revealed the larger contribution of the heavier and more polarizable center cations to NLO-property. $\text{BaGa}_2\text{SnSe}_6$ melts incongruently at a relative low temperature and the optical band gap is 1.95 eV. Besides, the calculated birefringence of $\text{BaGa}_2\text{SnSe}_6$ ($\Delta n = 0.1649$) for conventional $1.064 \mu\text{m}$ pumping laser is sufficiently large to achieve phase matching. Such a compound may arouse further interest in exploring new IR NLO materials with Sn or other heavy atoms.

Acknowledgments

This research was supported the National Natural Science Foundation of China (No.s 51472251, and 21271178).

References

- 1 D. M. Burland, R. D. Miller, and C. A. Walsh, *Chem. Rev.*, 1994, **94**, 31.
- 2 T. A. Driscoll, H. J. Hoffman, R. E. Stone, and P. E. Perkins, *J. Opt. Soc. Am. B*, 1986, **3**, 683.
- 3 G. D. Boyd, R. C. Miller, K. Nassau, W. L. Bond, and A. Savage, *Appl. Phys. Lett.*, 1964, **5**, 234.
- 4 C. T. Chen, B. C. Wu, A. Jiang, and G. You, *Sci. Sin. B*, 1985, **28**, 235.
- 5 W. G. Zou, M. K. Lu, F. Gu, Z. L. Xiu, S. F. Wang, and G. J. Zhou, *Opt. Mater.*, 2006, **28**, 988
- 6 C. T. Chen, Y. C. Wu, A. Jiang, B. C. Wu, G. You, R. Li, and S. J. Lin, *Opt. Soc. Am. B*, 1989, **6**, 616.
- 7 C. T. Chen, Z. Y. Xu, D. Q. Deng, J. Zhang, G. K. L. Wong, B. C. Wu, N. Ye, and D. Y. Tang, *Appl. Phys. Lett.*, 1996, **68**, 2930.
- 8 B. C. Wu, D. Y. Tang, N. Ye, and C. T. Chen, *Opt. Mater.*, 1996, **5**, 105.
- 9 C. T. Chen, N. Ye, J. Lin, J. Jiang, W. R. Zeng, and B. C. Wu, *Adv. Mater.*, 1999, **11**, 1071.
- 10 M. C. Ohmer, R. Pandey, and B. H. Bairamov, *MRS Bull.* 1998, **23**, 16.
- 11 A. Harasaki and K. J. Kato, *J. Appl. Phys.*, 1997, **36**, 700.
- 12 B. Tell and H. M. Kasper, *Phys. Rev. B*, 1971, **4**, 4455.
- 13 G. Airoldi, P. Beucherie and C. Rinaldi, *J. Cryst. Growth*, 1977, **38**, 239.
- 14 G. D. Boyd, E. Buehler and F. G. Storz, *Appl. Phys. Lett.*, 1971, **18**, 301.
- 15 P. G. Schunemann, K. L. Schepler, and P. A. Budni, *MRS Bull.* 1998, **23**, 45.

- 16 G. B. Jin, A. D. Raw, S. Skanthakumar, R. G. Haire, L. Soderholm, and J. A. Ibers, *J. Solid State Chem.*, 2010, **183**, 547.
- 17 J. Q. He, Z. Wang, X. Zhang, C. Cheng, Y. Gong, X. F. Lai, C. Zheng, J. H. Lin, and F. Q. Huang, *RSC Adv.*, 2015, **5**, 52629.
- 18 G. H. Zhang, H. J. Chen, Y. A. Xie, and F. Q. Huang, *CrystEngComm*, 2014, **16**, 1810.
- 19 G. B. Jin, E. S. Choi, R. P. Guertin, C. H. Booth, and T. E. Albrecht-Schmitt, *Chem. Mater.*, 2011, **23**, 1306.
- 20 A. J. Hong, L. Li, H. X. Zhu, Z. B. Yan, J.-M. Liu and Z. F. Renb, *J. Mater. Chem. A*, 2015, **3**, 13365.
- 21 G. Tan, F. Shi, J. W. Doak, H. Sun, L.-D. Zhao, P. Wang, C. Uher, C. Wolverton, V. P. Dravid, and M. G. Kanatzidis, *Energy Environ. Sci.* 2015, **8**, 267.
- 22 Q. Tan, L.-D. Zhao, J.-F. Li, C.-F. Wu, T.-R. Wei, Z.-B. Xing, and Kanatzidis, M. G. *J. Mater. Chem. A* 2014, **2**, 17302.
- 23 M. S. Devi, and K. Vidyasagar, *J. Chem. Soc., Dalton Trans.* 2002, **2092**.
- 24 I. Chung and M. G. Kanatzidis, *Chem. Mater.*, 2014, **26**, 849.
- 25 X. S. Lin, G. Zhang and N. Ye, *Cryst. Growth & Des.*, 2009, **9**, 1186.
- 26 J. Y. Yao, D. J. Mei, L. Bai, Z. S. Lin, W. L. Yin, P. Z. Fu and Y. C. Wu, *Inorg. Chem.*, 2010, **49**, 9212.
- 27 L. R. Dalton, P. A. Sullivan, and D. H. Bale, *Chem. Rev.* 2010, **110**, 25.
- 28 I. Chung, M. G. Kim, J. I. Jang, J. He, J. B. Ketterson, and M. G. Kanatzidis, *Angew. Chem., Int. Ed.* 2011, **50**, 10867.

- 29 I. Chung, J.-H. Song, J. I. Jang, A. J. Freeman, and M. G. Kanatzidis, *J. Solid State Chem.*, 2012, **195**, 161.
- 30 T. K. Bera, J. I. Jang, J. H. Song, C. D. Malliakas, A. J. Freeman, J. B. Ketterson, and M. G. Kanatzidis, *J. Am. Chem. Soc.*, 2010, **132**, 3484.
- 31 T. K. Bera, J. H. Song, A. J. Freeman, J. I. Jang, J. B. Ketterson, and M. G. Kanatzidis, *Angew. Chem., Int. Ed.* 2008, **47**, 7828.
- 32 S. Banerjee, C. D. Malliakas, J. I. Jang, J. B. Ketterson and M. G. Kanatzidis, *J. Am. Chem. Soc.*, 2008, **130**, 12270.
- 33 K. Feng, L. Kang, Z. Lin, J. Yao and Y. Wu, *J. Mater. Chem. C*, 2014, **2**, 4590.
- 34 K. Feng, X. Jiang, L. Kang, W. Yin, W. Hao, Z. Lin, J. Yao, Y. Wu and C. Chen, *Dalton trans.*, 2013, **42**, 13635.
- 35 W. L. Yin, K. Feng, W. Y. Hao, J. Y. Yao and Y. C. Wu, *Inorg. Chem.*, 2012, **51**, 5839.
- 36 W. L. Yin, K. Feng, R. He, D. J. Mei, Z. S. Lin, J. Y. Yao and Y. C. Wu, *Dalton Trans.*, 2012, **41**, 5653.
- 37 Z. Z. Luo, C. S. Lin, H. H. Cui, W. L. Zhang, H. Zhang, Z. Z. He and W. D. Cheng, *Chem. Mater.*, 2014, **26**, 2743.
- 38 X. S. Li, L. Kang, C. Li, Z. S. Lin, J. Y. Yao, and Y. C. Wu, *J. Mater. Chem. C* 2015, **3**, 3060.
- 39 Z. H. Lin, C. Li, L. Kang, Z. S. Lin, J. Y. Yao, and Y. C. Wu, *Dalton Trans.*, 2015, **44**, 7404.
- 40 C. Chen, Z. Lin, and Z. Wang, *Appl. Phys. B: Lasers Opt.* 2005, **80**, 1.

- 41 CrystalClear. Rigaku Corporation: Tokyo, Japan, 2008.
- 42 G. M. Sheldrick, *Acta Crystallogr. A*, 2008, **64**, 112.
- 43 L. M. Gelato, and E. J. Parthé *Appl. Crystallogr.* 1987, **20**, 139.
- 44 S. K. Kurtz and T. T. Perry, *J. Appl. Phys.*, 1968, **39**, 3798.
- 45 S. J. Clark, M. D. Segall, C. J. Pickard, P. J. Hasnip, M. J. Probert, K. Refson and M. C. Payne, *Z. Kristallogr.*, 2005, **220**, 567.
- 46 J. S. Lin, A. Qteish, M. C. Payne and V. Heine, *Phys. Rev. B*, 1993, **47**, 4174.
- 47 D. M. Ceperley and B. J. Alder, *Phys. Rev. Lett.*, 1980, **45**, 566.
- 48 H. J. Monkhorst and J. D. Pack, *Phys. Rev. B*, 1976, **13**, 5188.
- 49 R. W. Godby, M. Schluter, and L. J. Sham, *Phys. Rev. B*, 1988, **37**, 10159.
- 50 C. S. Wang, B. M. Klein, *Phys. Rev. B*, 1981, **24**, 3417.
- 51 J. Lin, M. H. Lee, Z. P. Liu, C. T. Chen, and C. J. Pickard, *Phys. Rev. B*, 1999, **60**, 13380.
- 52 V. B. Ghanwat, S. S. Mali, R. M. Mane, P. S. Patil, C. K. Hong and P. N. Bhosale, *New J. Chem.*, 2015, **39**, 5661.
- 53 X. X. Zhang, F. Lou, C. L. Li, X. Zhang, N. Jia, T. T. Yu, J. L. He, B. T. Zhang, H. B. Xia, S. P. Wang, and X. T. Tao, *CrystEngComm*, 2015, **17**, 4026.
- 54 C. M. Thompson, K. Kovnir, V. O. Garlea, E. S. Choi, H. D. Zhou and M. Shatruk, *J. Mater. Chem. C*, 2014, **2**, 7561.
- 55 S.-J. Hwang, R. G. Iyer, and M. G. Kanatzidis, *J. Solid State Chem.*, 2004, **177**, 3640.

- 56 X. Chen, X. Y. Huang, A. H. Fu, J. Li, L. D. Zhang and H. Y. Guo, *Chem. Mater.*, 2000, **12**, 2385.
- 57 W. Yin, Z. Lin, L. Kang, B. Kang, J. Deng, Z. Lin, J. Yao and Y. Wu, *Dalton trans.*, 2015, **44**, 2259.
- 58 S.-M. Kuo, Y.-M. Chang, I. Chung, J.-I. Jang, B.-H. Her, S.-H. Yang, J. B. Ketterson, M. G. Kanatzidis and K.-F. Hsu, *Chem. Mater.*, 2013, **25**, 2427.
- 59 Z.-Z. Luo, C.-S. Lin, H.-H. Cui, W.-L. Zhang, H. Zhang, H. Chen, Z.-Z. He and W.-D. Cheng, *Chem. Mater.*, 2015, **27**, 914.
- 60 C. Aydın, M. S. Abd El-sadek, K. Zheng, I. S. Yahia and F. Yakuphanoglu, *Opt. Laser Technol.*, 2013, **48**, 447.
- 61 E. L. Simmons, *Appl. Opt.*, 1975, **14**, 1380.
- 62 D. J. Mei, P. F. Gong, Z. S. Lin, K. Feng, J. Y. Yao, F. Q. Huang, and Y. C. Wu, *CrystEngComm*, 2014, **16**, 6836.
- 63 M. H. Lee, C. H. Yang and J. H. Jan, *Phys. Rev. B*, 2004, **70**.

Fig. captions

Fig. 1. Experimental (red) and simulated (black) X-ray powder diffraction data of $\text{BaGa}_2\text{SnSe}_6$.

Fig. 2. (A) Coordination environments of all cations in $\text{BaGa}_2\text{SnSe}_6$. (B) A single $(\text{Ga/Sn})_3\text{Se}_9$ layer perpendicular to the c direction with a single $(\text{Ga/Sn})_3\text{Se}_9$ group marked by a red circle. (C) Crystal packing structure of $\text{BaGa}_2\text{SnSe}_6$ viewed down the b -axis with the unit cell marked.

Fig. 3. The DSC pattern of $\text{BaGa}_2\text{SnSe}_6$.

Fig. 4. Optical reflection spectrum of $\text{BaGa}_2\text{SnSe}_6$.

Fig. 5. Phase-matching curves of $\text{BaGa}_2\text{SnSe}_6$.

Fig. 6. Oscilloscope traces of SHG signals for $\text{BaGa}_2\text{SnSe}_6$ with AgGaS_2 as a reference at a particle size of 105~150 μm .

Fig. 7. The total and partial density of states (DOS and PDOS, respectively) of $\text{BaGa}_2\text{SnSe}_6$. Dashed line represents the Fermi energy (E_f).

Table 1. Crystal data and structure refinement for BaGa₂SnSe₆

	BaGa ₂ SnSe ₆
fw	869.23
T (K)	153
<i>a</i> (Å)	10.1449(14)
<i>c</i> (Å)	9.2490(18)
space group	<i>R</i> 3
<i>V</i> (Å ³)	824.4(2)
<i>Z</i>	3
ρ_c (g cm ⁻³)	5.253
μ (cm ⁻¹)	30.431
<i>R</i> (<i>F</i>) ^a	0.0228
<i>R</i> _w (<i>F</i> _o ²) ^b	0.0413

^a*R*(*F*) = $\sum||F_o| - |F_c|| / \sum|F_o|$ for $F_o^2 > 2\sigma(F_o^2)$. ^b*R*_w(*F*_o²) = $\{\sum[w(F_o^2 - F_c^2)^2] / \sum w F_o^4\}^{1/2}$ for all data. $w^{-1} = \sigma^2(F_o^2) + (zP)^2$,

where $P = (\text{Max}(F_o^2, 0) + 2 F_c^2) / 3$ $z = 0.09$.

Table 2. Selected bond lengths (\AA) for $\text{BaGa}_2\text{SnSe}_6$

Ba–Se1 $\times 3$	3.8131(9)	Ba–Se21	3.5892(9)
Ba–Se1 $\times 2$	3.6600(7)	Ga/Sn–Se1	2.4355(7)
Ba–Se1	3.6601(7)	Ga/Sn–Se1	2.4373(7)
Ba–Se2 $\times 2$	3.8103(7)	Ga/Sn–Se2	2.4385(8)
Ba–Se2 $\times 2$	3.8591(9)	Ga/Sn–Se2	2.4501(7)
Ba–Se2	3.8102(7)		

Table 3. The refractive indices and birefringence of BaGa₂SnSe₆.

λ (nm)	1064	2090
n_x	3.2170	3.1077
n_y	3.2425	3.1319
n_z	3.0776	2.9846
Δn	0.1649	0.1473

Table 4. The NLO coefficients of BaGa₂SnSe₆.

NLO coefficients (pm/V)			
d ₁₁	62.91	d ₁₆	-30.66
d ₁₂	-9.33	d ₂₂	2.8
d ₁₃	-11.39	d ₂₃	36.59
d ₁₄	-16.55	d ₂₄	-20.26
d ₁₅	11.6	d ₃₃	50.26
Powder			
		40.06	
SHG			

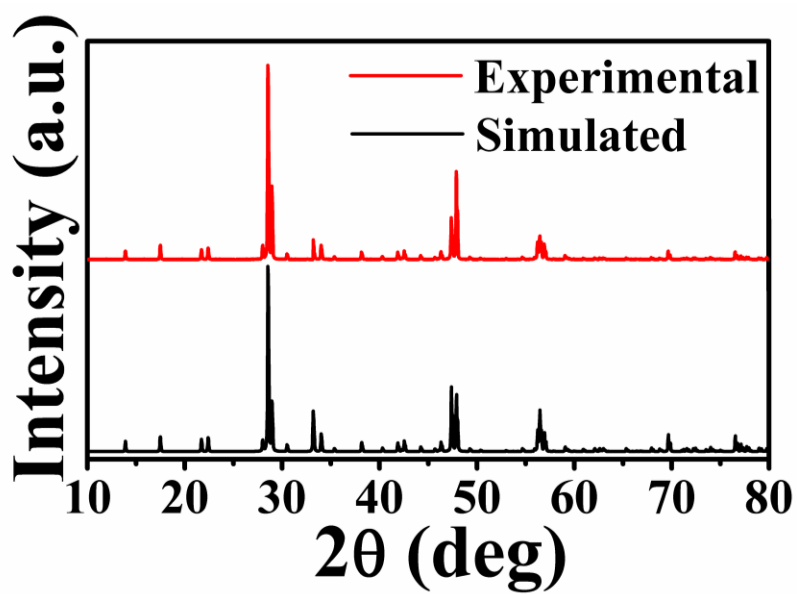


Fig. 1. Experimental (red) and simulated (black) X-ray powder diffraction data of $\text{BaGa}_2\text{SnSe}_6$.

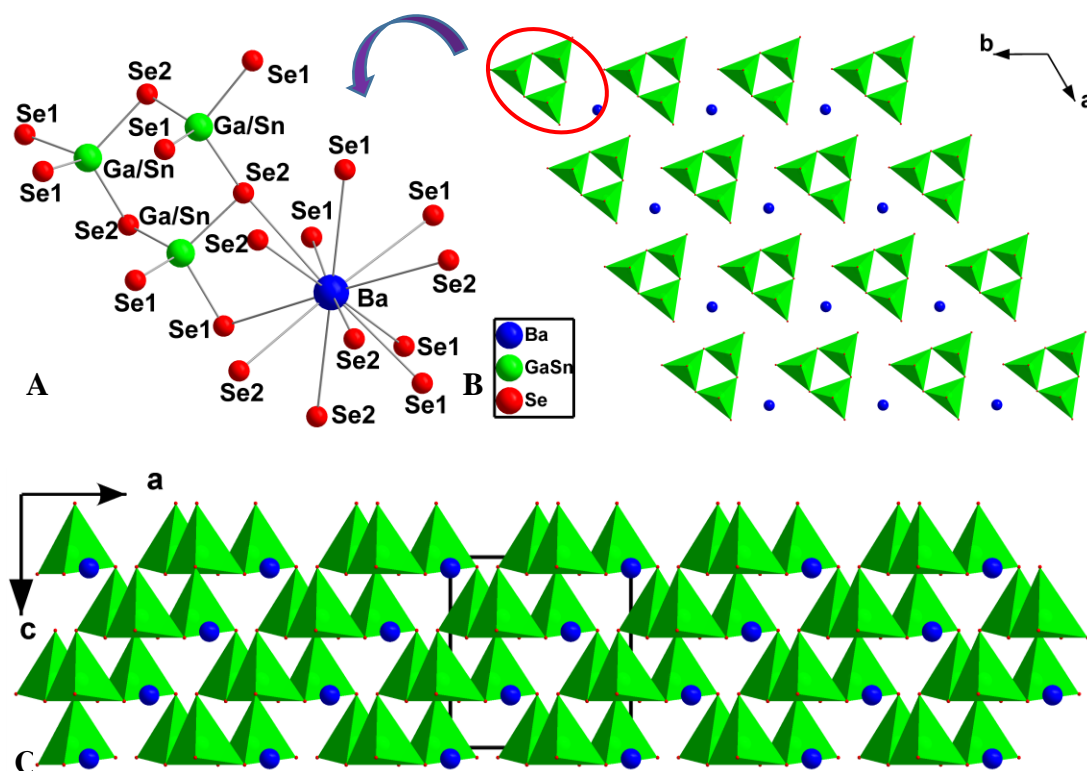


Fig. 2. (A) Coordination environments of all cations in BaGa₂SnSe₆. (B) A single (Ga/Sn)₃Se₉ layer perpendicular to the *c* direction with a single (Ga/Sn)₃Se₉ group marked by a red circle. (C) Crystal packing structure of BaGa₂SnSe₆ viewed down the *b*-axis with the unit cell marked.

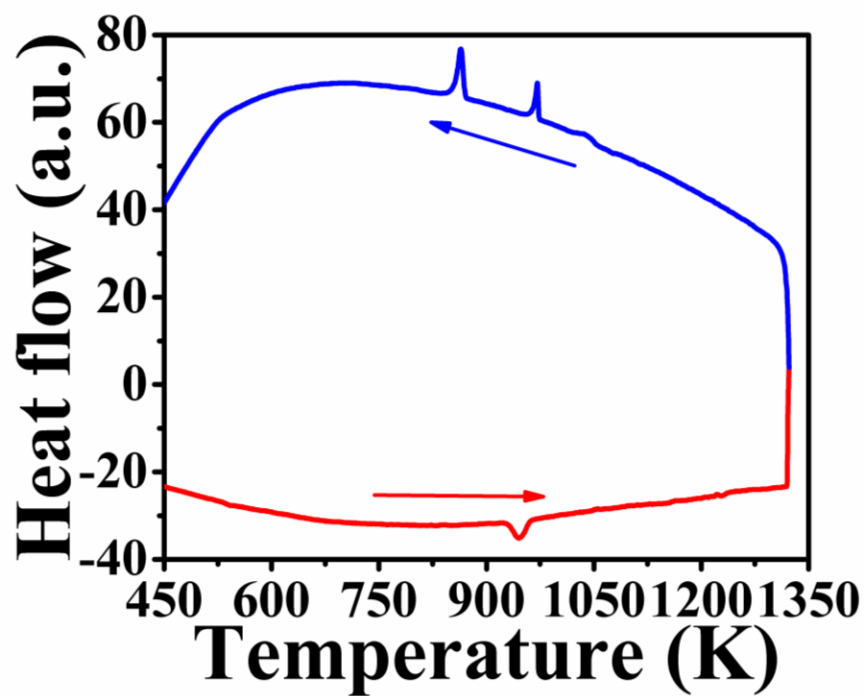


Fig. 3. The DSC pattern of BaGa₂SnSe₆.

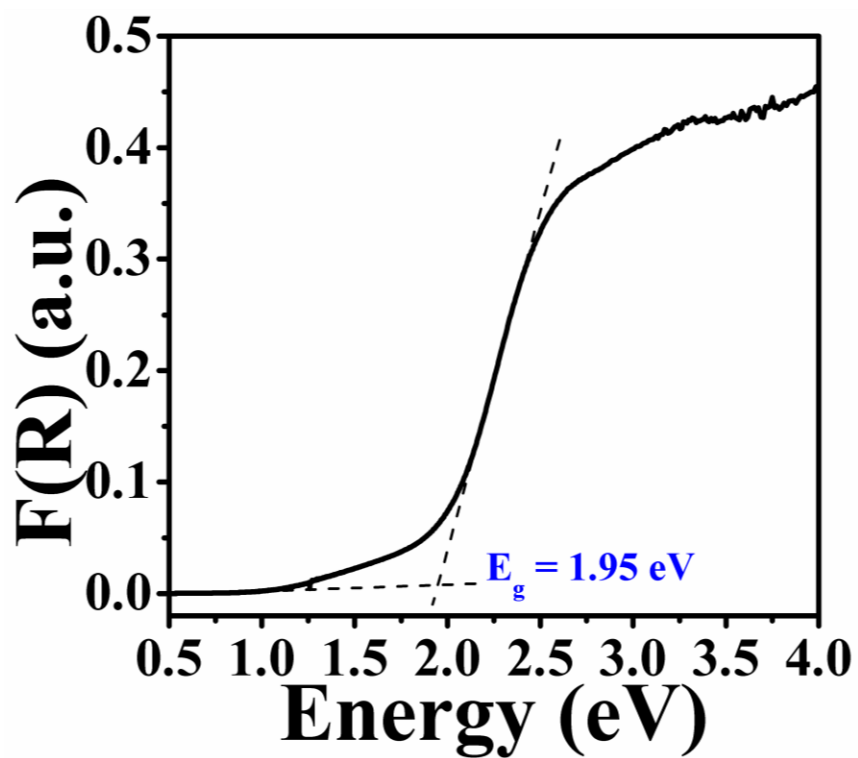


Fig. 4. Optical reflection spectrum of BaGa₂SnSe₆.

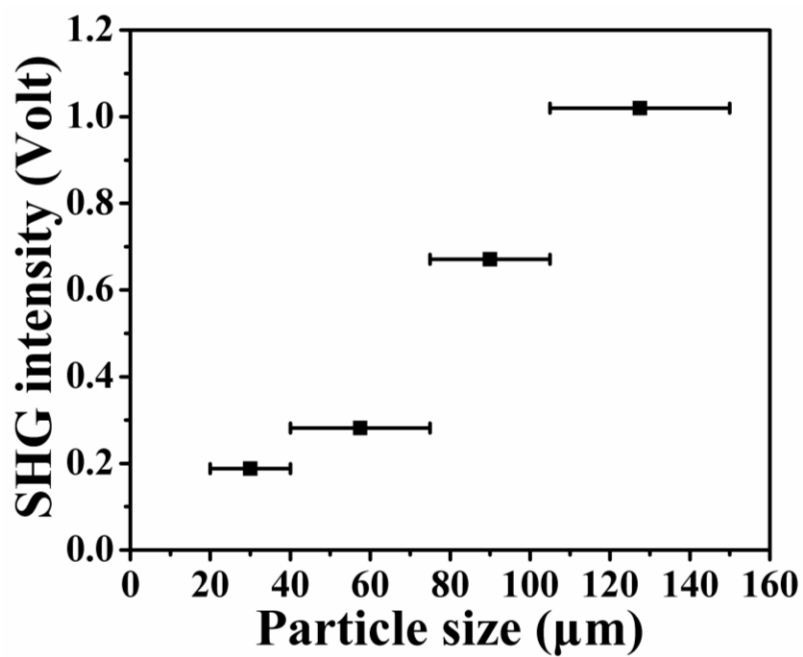


Fig. 5. Phase-matching curves of BaGa₂SnSe₆.

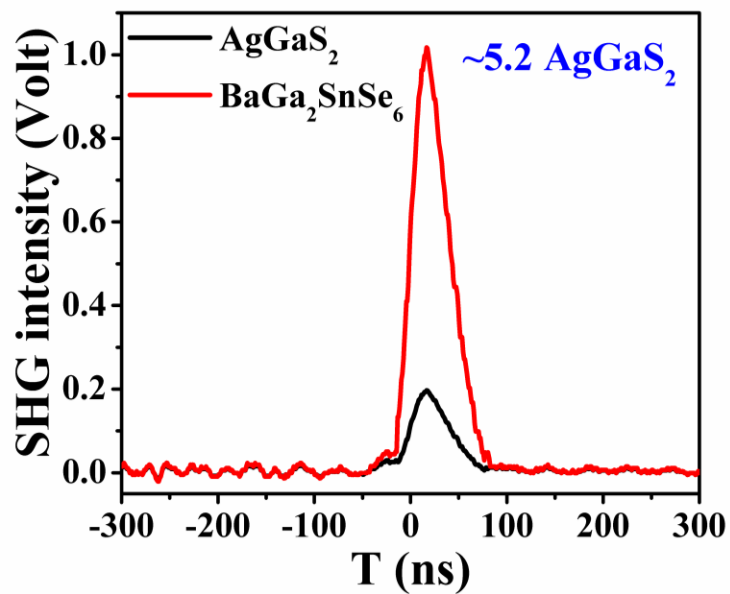


Fig. 6. Oscilloscope traces of SHG signals for BaGa₂SnSe₆ with AgGaS₂ as a reference at a particle size of 105~150 μm .

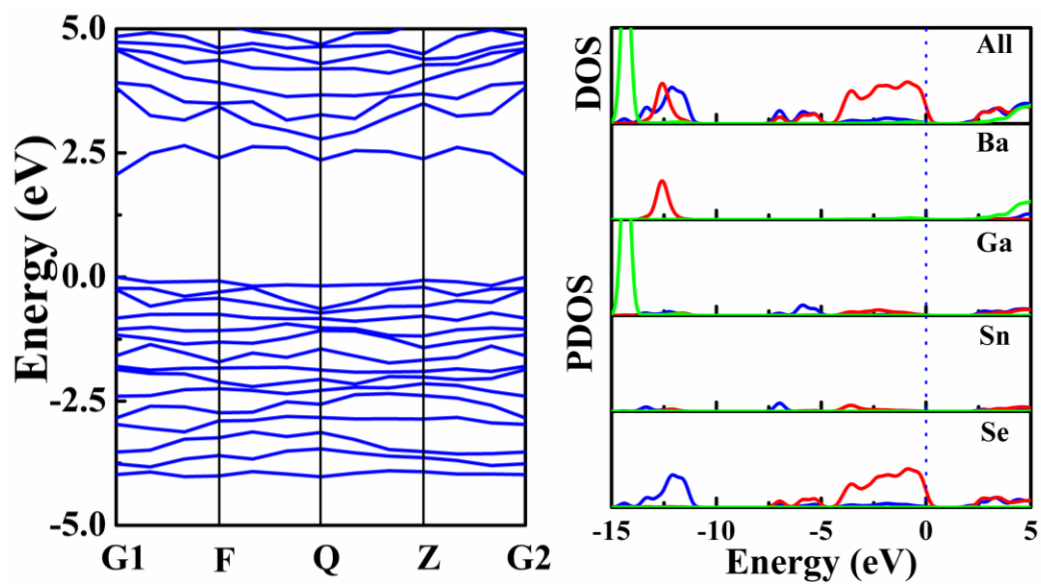


Fig. 7. The band structure and the total and partial density of states (DOS and PDOS, respectively) of $\text{BaGa}_2\text{SnSe}_6$. Dashed line represents the Fermi energy (E_f).

Table of Contents Entry

BaGa₂SnSe₆ exhibits a very strong NLO response ~ 5.2 AgGaS₂ and shows type-I phase-matchable behavior.

